INTERNATIONAL TABLES FOR CRYSTALLOGRAPHY

ISSN 1574-8707
it.iucr.org

Volume I, X-ray Absorption Spectroscopy and Related Techniques
ISBN: 978-1-119-43394-1

Chapter 3.47

Keywords: X-ray absorption spectroscopy; X-ray extended-range technique; projected roughness.

Projected roughness in X-ray absorption spectroscopy

Martin D. de Jonge,[a]* Christopher T. Chantler[b] and Chanh Q. Tran[c]

[a]Australian Synchrotron, ANSTO, Clayton, Australia, [b]School of Physics, University of Melbourne, Victoria 3010, Australia, and [c]Department of Mathematical and Physical Sciences, La Trobe University, La Trobe, Victoria 3086, Australia. *Correspondence e-mail: martind@ansto.gov.au

The characterization of samples is critical to all X-ray absorption spectroscopy (XAS) measurements, whether seeking calibrated data for comparison with advanced theory or relative data for fingerprinting analysis via methods such as principal component analysis or linear combination fitting. For solids, the thickness, thickness profile and integrated column density are relevant. More subtle but similar is where the beam intersects a variable projected thickness of the sample. In this chapter, this variation of the projected thickness is defined and the name *the projected roughness* is suggested. This projected roughness causes changes to the structure of the near-edge XAS and pre-edge and X-ray absorption near-edge structure (XANES) in particular. Included in this concept is local heterogeneity, which includes the variation of local composition across a sample, whether thickness, mass density or nanostructure. The impact of projected roughness scales with the mass attenuation coefficient and so will be most pronounced at low photon energies or high atomic number, where tabulations show the greatest divergence. It is demonstrated that projected roughness can easily affect the X-ray absorption fine-structure oscillations by 2% or more, especially in an energy-dependent functional in the XANES region. It therefore affects the applicability of advanced theory to predict XAS spectra. Projected roughness can compromise the fingerprinting of a reference material or unknown in pre-edge structure and can affect the first part of XANES for matching to unknowns or for principal component analysis and related approaches. The impact of projected roughness can be used to characterize the effect and it can be corrected to improve measurement accuracy, theoretical structure identification and intercomparability.

1. Introduction

The mass attenuation coefficient reflects the transition probability of a simple atomic system interacting with an incident X-ray. In the 0.1–100 keV range, the energy dependence of the mass attenuation coefficient is strongly influenced by the absorption edge from the detailed configuration of the atomic orbitals and the local chemical environment. Accurate measurement is used to provide tests of atomic theory and calculation methods, and data ranging from absolutely scaled to relative can probe the orbital density of states via X-ray absorption near-edge structure (XANES) and the local chemical environment via extended X-ray absorption fine structure (EXAFS).

We will show that the projected roughness affects local oscillations, amplitudes and X-ray absorption fine structure (XAFS). As such, it affects both relative accuracy and precision and is relevant for any high-accuracy measurement. Since the projected roughness can impact local (XAFS) structure and amplitudes by 2% and more (Glover *et al.*, 2009), the effect is important if these amplitudes are used for principal

Related chapters

Volume I: 3.12, 3.13, 3.14, 3.39, 3.41, 3.42, 3.43, 3.46, 4.3, 4.6, 4.7, 5.9

component analysis or related techniques or for XAFS fitting of paths within some Hanning window. The effect of projected roughness is substantial for the pre-edge and the first few XAFS oscillations; however, if one excludes these from the Hanning window then the effect of projected roughness may sometimes not affect the fitting parameters.

In this chapter, we concentrate on the effect of the variation in local projected thickness (*i.e.* the projected roughness) in X-ray transmission across the sample at a lateral length scale that is below the size of the probe beam and show that this can have a detrimental impact on both absolute and relatively scaled measurements, with particular caution to measurements in the tender X-ray regime.

In order to advance these arguments, we generalize the concept of roughness as a measure of surface variations into the projected specimen domain to include variations in the integrated column density. Projected roughness can be divided into surface roughness, as perhaps measured by a profilometer or scanning electron microscope, destructively or nondestructively, and internal 'roughness', such as at an interfacial layer, in a multilayer, at domain or phase boundaries, or density variations resulting from internal vacuoles or deposition packing mechanics. Projected roughness hence includes such complexity of origin in both measurement and theory. X-ray transmission techniques enable us to measure and investigate both surface and internal roughness. X-ray absorption is affected by any change in composition or density and hence can be used to observe and measure any variation in integrated column density.

Several articles in this volume relate to thickness effects and hence to this general area of inquiry, and we point to these chapters for a variety of important details and comments (Bunker, 2024*a*,*b*; Bridges, 2024; De Panfilis & Bardelli, 2024). An excellent text (Bunker, 2010) discusses thickness effects (Chapter 3.6.5, pp. 87–88), including the existence of roughness and sample non-uniformity. In this chapter, we are not interested so much in how to mount powders and solids (Bunker, 2024*a*), which might yield larger or smaller uniformity, heterogeneity and loss of stress, nor in a general discussion of samples for XAS (Bunker, 2024*a*), nor in the complex variety of thickness effects (Bridges, 2024), nor directly in the loss of spectral information and amplitudes from bandwidth and divergence (Bunker, 2024*b*), all of which are important, but in the diagnosis and mapping of the consequences of sample heterogeneity across the X-ray beam. That is, this chapter is concerned with observing, diagnosing and correcting the impact on the near-edge structure resulting from the projected roughness of the sample.

This chapter presents a definition of the projected roughness, investigations of the effect of the projected roughness on measurements of X-ray mass attenuation coefficients, accurate physical models of this effect, illustration through two case studies and a discussion of particular scenarios in which the effect will be significant. We illustrate through measurements mass attenuation coefficients $[\mu/\rho]$ which show unique signatures due to projected roughness. In addition to correcting a systematic error in the determination of the mass attenuation coefficient, the study defines and provides nondestructive techniques for determining the magnitude of the projected roughness.

2. Definition

The term roughness is generally understood as relating to the root-mean-square (r.m.s.) variations in the surface height. The roughness distribution can likewise be understood in this context as relating to the distinct form of the surface variations: triangular, Gaussian, top hat *etc.* Thus, when a projected measurement is undertaken, the usual statistical mathematics are applied to the roughness that comes from the front and rear surface. However, in a transmission measurement, in the absence of significant refraction or diffraction through the specimen, the integrated column density $[\rho t]$ is the relevant parameter (Chantler *et al.*, 2004; Bunker, 2010):

$$[\rho t](x, y) = \int_{\mathbb{P}} \rho(\mathbf{r})\, \mathrm{d}z. \tag{1}$$

Here, $\mathbb{P}$ is the path of a single ray of an X-ray beam for normal incidence, through a point at (x, y) on the specimen, with z parallel to the beam axis. $\rho(\mathbf{r})$ is the density of the sample at the point $\mathbf{r} = (x, y, z)$. The square brackets in equation (1) are used to signify that the integrated column density $[\rho t]$ is a single object, as distinct from the product of density ρ and thickness t (de Jonge *et al.*, 2004*a*). We treat the mass attenuation coefficient $[\mu/\rho]$ similarly. Whilst $\rho(\mathbf{r})$ is far from experimentally accessible, and t is normally accessible in a macroscopic sense, $[\rho t]$ is far more experimentally accessible and is easily determined for foils using $\overline{[\rho t]} = m/A$, where m is the mass and A is the perpendicular area. We have shown elsewhere (de Jonge *et al.*, 2004*b*) that $[\rho t](x, y)$ can be determined by combining $\overline{[\rho t]}$ with X-ray absorption measurements made across the entire surface of a foil. With this definition, we will drop the positional reference for the integrated column density, so that $[\rho t] \equiv [\rho t](x, y)$.

When the integrated column density is used, the concept of roughness needs to be generalized from a surface-only parameter to the projected bulk. Interestingly, we have found no established quantity for this, and have considered terms such as 'bulk roughness' and 'the r.m.s. of the projected density', but find none particularly satisfying. On the other hand, the term 'roughness' is often used with an exclusive intent as 'surface roughness' and too easily hides the scope and importance of the new parameter. Accordingly, we here adopt the term 'projected roughness' (symbol $\sigma_{[\rho t]}$) to distinguish it from the surface roughness σ_t, and define it using the usual convention of r.m.s. deviations,

$$\sigma_{[\rho t]} = \left(\frac{1}{A} \int_{\mathbb{S}} ([\rho t] - \overline{[\rho t]})^2 \, \mathrm{d}x \, \mathrm{d}y \right)^{1/2}, \tag{2}$$

where $\mathbb{S}$ is a finite region of the specimen with area A.

3. Theory

3.1. Projected roughness

The effect of projected roughness on the measurement of attenuation appears to have been described first by Goulon *et al.* (1982), and more recently by Tran *et al.* (2004) and de Jonge *et al.* (2004*b*), but none of these studies observed the effect. It has been discussed in the context of the X-ray extended-range technique (XERT; Chantler *et al.*; 2001) and high-accuracy measurements (de Jonge *et al.*, 2005, 2007). The work of Boster (1973) and others has described the impact of various thickness profiles (wedges, for example) to yield a correction to the measured attenuation, but these specific thickness distributions lead to a significantly less general interpretation of the effect and do not treat internal and void structures.

Here, we follow the derivation of de Jonge (2005). Alternative and equivalent derivations can be found in Goulon *et al.* (1982), Tran *et al.* (2004) and Glover *et al.* (2009), and a similar expansion is given in Bunker (2010). For an incident beam $I_0 = I_0(x, y)$ of cross-sectional area A, the transmitted intensity I is given by

$$I = \frac{1}{A}\int_{\mathbb{S}} I_0 \exp\{-[\mu/\rho][\rho t]\}\,\mathrm{d}x\,\mathrm{d}y. \tag{3}$$

The intensity profile of the incident beam does not generally impact this discussion as long as it is not correlated with the structure in $[\rho t]$, and so we factor it out of the integral and perform a Taylor series expansion of the integrand around $\overline{[\rho t]}$ to give

$$\begin{aligned}\frac{I}{I_0} &= \frac{1}{A}\exp\{-[\mu/\rho]\overline{[\rho t]}\}\int_{\mathbb{S}} \exp\{-[\mu/\rho]([\rho t]-\overline{[\rho t]})\}\,\mathrm{d}x\,\mathrm{d}y\\ &= \frac{1}{A}\exp\{-[\mu/\rho]\overline{[\rho t]}\}\int_{\mathbb{S}}\left\{1-[\mu/\rho]([\rho t]-\overline{[\rho t]})\right.\\ &\quad\left.+\ \frac{[\mu/\rho]^2([\rho t]-\overline{[\rho t]})^2}{2!}+\ldots\right\}\mathrm{d}x\,\mathrm{d}y.\end{aligned}$$

The second term in the integral identically contributes zero. The third term invokes the projected roughness defined in equation (2) and so

$$\begin{aligned}\frac{I}{I_0} &\simeq \exp\{-[\mu/\rho]\overline{[\rho t]}\}\left(1+\frac{[\mu/\rho]^2\sigma^2_{[\rho t]}}{2}\right)\\ &\simeq \exp\left[-[\mu/\rho]\overline{[\rho t]}\left(1-\frac{[\mu/\rho]\sigma^2_{[\rho t]}}{2\overline{[\rho t]}}\right)\right].\end{aligned} \tag{4}$$

These expressions for the intensity ratio are valid for small values of the projected roughness $\sigma_{[\rho t]}$. The fractional impact on the mass attenuation coefficient due to the effect of the projected roughness is therefore

$$\begin{aligned}\frac{[\mu/\rho]_m-[\mu/\rho]}{[\mu/\rho]} = \frac{\Delta_{[\mu/\rho]}}{[\mu/\rho]} &\simeq \frac{-[\mu/\rho]\sigma^2_{[\rho t]}}{2\overline{[\rho t]}} = \frac{-1}{2}[\mu/\rho]\left(\frac{\sigma_{[\rho t]}}{\overline{[\rho t]}}\right)\sigma_{[\rho t]}\\ &= \frac{1}{2}\ln(I/I_0)\left(\frac{\sigma^2_{[\rho t]}}{\overline{[\rho t]}}\right)^2,\end{aligned} \tag{5}$$

where $[\mu/\rho]_m = (-1/\overline{[\rho t]})\ln(I/I_0)$ is the value that would be determined without consideration of the effect of the projected roughness.

3.2. Correlation: integrated column density

The signature of the effect of projected roughness [*i.e.* the variation of $[\rho t]$ in the (x, y) plane] is partly correlated with that of an error in the integrated column density $[\rho t]$ [*i.e.* the integral of the density $\rho(\mathbf{r})$ through the thickness z] and therefore the two effects must be resolved simultaneously (de Jonge *et al.*, 2005; Glover *et al.*, 2009, 2010; Ekanayake *et al.*, 2021*a*). As the Beer–Lambert law contains only the product of $[\mu/\rho]$ and $[\rho t]$, the fractional error in the mass attenuation coefficient $[\mu/\rho]$ resulting from an error $\Delta_{[\rho t]}$ in the employed value of the integrated column density $[\rho t]$ is given by

$$\frac{\Delta_{[\mu/\rho]}}{[\mu/\rho]} = \frac{-\Delta_{[\rho t]}}{[\rho t]}. \tag{6}$$

We will use this equation later in our discussion of the effect of projected roughness.

4. Discussion of the formula

According to equation (4), the apparent integrated column density obtained by using attenuation measurements with a known $[\mu/\rho]$ is smaller than the linearly averaged integrated column density within the beam footprint by the amount $\frac{1}{2}[\mu/\rho]\sigma^2_{[\rho t]}$. Equivalently, when the integrated column density $[\rho t]$ within the beam footprint is determined by linear averaging (for example, by using $\overline{[\rho t]} = m/A$), measurements of the attenuation coefficients are overestimated by this factor. Hence, the linearly averaged column density should not be used in the Beer–Lambert relation to determine mass attenuation coefficients.

Equation (5) tells us that the fractional impact of the projected roughness scales with $[\mu/\rho]$ and so is not constant across an X-ray spectrum. The fractional impact increases with the mass attenuation coefficient. As a result, the impact cannot be removed by scaling the spectrum data, and so roughness impacts both relative and absolute measurements alike. Specifically, for principal component analysis (PCA), linear combination fitting (LCF) and fingerprinting studies, samples measured with different roughnesses and with different attenuations cannot be compared beyond the level of the impact of the projected roughness. Spectral distortion due to projected roughness will be falsely accommodated by other components that are not actually present in a specimen. For EXAFS methods, spectral distortion will result in peak suppression that will also distort estimates of the Debye–Waller factor, bond length and coordination number, also compromising these methods.

The impact of the disturbance on XAS methods may depend further on the method employed. XANES measurements, by their nature, probe a substantial range of $[\mu/\rho]$ and so will be strongly affected. EXAFS measurements, as well as being critically sensitive to above-edge oscillations, may also

rely on below-edge and edge-step normalizations, which can still result in significant distortion of data from different specimens.

Absolute data will always be impacted by projected roughness effects, in accordance with equations (4) and (5). However, use of the X-ray extended-range technique (Chantler *et al.*, 2001) to provide measurements over a wide range of $[\mu/\rho]$ can enable the clear identification and correction of the effect. When measurements are made at a single energy (*i.e.* with a single value of $[\mu/\rho]$) it is impossible to resolve between an incorrect value of $[\rho t]$ (equation 6) and the effect of projected roughness (equation 5). As a result, the absolute measurement will suffer an unidentifiable, and hence uncorrectable, systematic error.

What is the typical magnitude of the effect? This is difficult to answer in the abstract. However, we consider the case of a relatively scaled measurement across an absorption edge. We consider a specimen selected with negative log attenuation of 2, which is the Nordfors recommended ideal for a single XAFS measurement (Nordfors, 1960). Then, $-\ln(I/I_0) = [\mu/\rho][\rho t] \simeq 2$ and equation (5) becomes

$$\frac{\Delta_{[\mu/\rho]}}{[\mu/\rho]} \simeq -\left(\frac{\sigma_{[\rho t]}}{[\rho t]}\right)^2. \qquad (7)$$

In this situation, at a single energy, the fractional effect is proportional to the square of the fractional projected roughness, and a 10% projected roughness results in a 1% effect on the mass attenuation coefficient, independent of all other parameters.

At present, we are aware of three nominally equivalent methods for determining $\sigma_{[\rho t]}$ and a correction to the mass attenuation coefficients:

(i) Track the systematic discrepancy in $[\mu/\rho]$ between thin and thick specimens as a function of the X-ray energy E (as in de Jonge *et al.*, 2005, 2007; Glover *et al.*, 2009, 2010); model the impact along with $[\rho t]$ errors and apply corrections to minimize the systematic discrepancies.

(ii) Plot $\Delta_{[\mu/\rho]}$ versus $[\mu/\rho]$; fit the quadratic and linear terms to determine $\sigma_{[\rho t]}$ and $[\rho t]$ simultaneously (Ekanayake *et al.*, 2021*b*).

(iii) Plot $\Delta_{[\mu/\rho]}/[\mu/\rho]$ versus $[\mu/\rho]$; fit the linear and offset terms to determine $\sigma_{[\rho t]}$ and $[\rho t]$ simultaneously (not yet demonstrated).

5. Correction for projected roughness

Early precise studies showed micro-structure from profilometry for copper in the range 200–600 nm for samples of thickness from 10 to 100 µm, with structure at lateral length scales of 10–100 µm. No strong roughness effect was explicitly diagnosed in the measurements of copper (8.85–20 keV; Chantler *et al.*, 2001) or silicon (5–20 keV; Tran *et al.*, 2003) despite these strong profilometry signatures, but it is likely that the signature of the effect was overwhelmed by other measurement uncertainties.

Follow-up investigations of projected roughness for molybdenum (13.5–41.5 keV; de Jonge *et al.*, 2005) and tin (29–60 keV; de Jonge *et al.*, 2007) found no observable roughness. In hindsight, the absence of the effect was due to the measurement with large thicknesses (25–250 µm for molybdenum; 25–500 µm for tin) and relatively smooth surfaces. Nonetheless, rolling defects and structural thickness changes of order 100 nm were observed using full-foil mapping with steps of 1 mm across the surface (de Jonge *et al.*, 2004*b*). The anticipated projected roughness signatures for these data sets were well below the measurement precision.

Projected roughness was first observed and quantified by Glover *et al.* (2009) and corrections were applied in Glover *et al.* (2010) and Ekanayake *et al.* (2021*a*). In all cases, observation was only possible due to use of the XERT (Chantler *et al.*, 2001) by probing an extended range of attenuation and energy space throughout the measurement. Here we outline the approach and findings of Glover *et al.* (2009) and Ekanayake *et al.* (2021*a*).

In Glover *et al.* (2009), projected roughness was measured for thin gold foils of nominal thickness 5 µm. Equation (5) relates $\sigma_{[\rho t]}$, $[\mu/\rho]$ and $[\rho t]$ to the change in measured mass attenuation coefficient ($\Delta_{[\mu/\rho]}$) for the thinner specimen. We approximate $\Delta_{[\mu/\rho]}$ by comparing it with measurement from a thicker specimen, noting that the impact of the projected roughness is reduced in proportion to the thickness, as discussed in Section 4.

The magnitude of the integrated column density and the projected roughness in the sample were fitted as $[\rho t] = 10.287 \pm 0.007$ mg cm^{-2} and $\sigma_{[\rho t]} = 1.276 \pm 0.033$ mg cm^{-2}, respectively. The best-fit model of the roughness discrepancy is compared with the experimental discrepancy in Fig 1. The agreement between the two is excellent. Note that equation (6) shows that an error in $[\rho t]$ would result in a constant fractional change to $[\mu/\rho]$ that is independent of the value of $[\mu/\rho]$, and so would only impact the vertical location of this

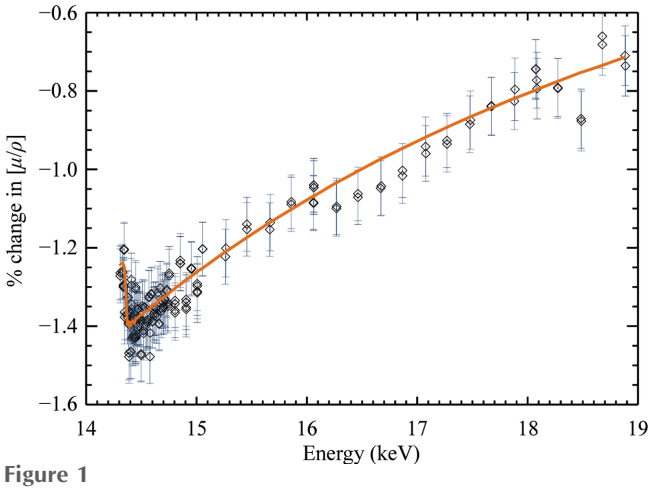

Figure 1
A comparison of the output of the roughness model (orange line) with the experimental discrepancy (diamonds with error bars), here defined as the fractional difference in the determined value of $[\mu/\rho]$ between the nominal 5 µm sample and the thicker samples. The roughness is thus determined to be $\sigma_{[\rho t]} = 1.276$ mg cm^{-2}, around 12.4% of $[\rho t]$.

curve if a correction for the projected roughness was not included.

The fractional projected roughness, *i.e.* the ratio of the projected roughness to the integrated column density across the area of the X-ray beam, was $\sigma_{[\rho t]}/[\rho t] = 0.124$, or 12.4%. If we assume that the gold foil has a uniform density of 19.30 g cm^{-3}, this corresponds to a thickness equivalent of $t = [\rho t]/\rho_{\rm nominal} = 5.330 \pm 0.004$ µm and a thickness equivalent roughness of $\sigma_t = \sigma_{[\rho t]}/\rho_{\rm nominal} = 661 \pm 17$ nm. The impact on the determined $[\mu/\rho]$ was up to 1.4%, as shown in Fig. 1; this impact can be applied as a correction to the measured values to improve their precision and overall accuracy.

It is interesting to also consider the approach of Ekanayake *et al.* (2021*a*), in which the projected roughness was characterized and used to correct the measurement of mass attenuation coefficients for zinc between 8.51 and 11.59 keV, spanning the *K*-shell absorption edge. Fig. 2 shows the difference between the measured value for a nominal 10 µm foil and that of a thicker 50 µm foil. The 50 µm foil can be used as a zero reference for roughness in this case as the impact of the roughness is one fifth that of the 10 µm foil, presuming similar levels of $\sigma_{[\rho t]}$ in both foils.

Fig. 2 includes a red line that indicates the approximate result of a fit with roughness fixed at $\sigma_{[\rho t]} = 0$. This demonstrates the measurement space that needs to be probed. The linear fit might seem quite reasonable, except that (i) it misses the clear second-order curvature term and (ii) it determines an incorrect value of $[\rho t]$, and hence an incorrect value of $[\mu/\rho]$, thereby resulting in a substantial offset in the determined values. Indeed, the $[\rho t]$ error that results from ignoring the effect of projected roughness can be estimated by equating the two contributions (equations 5 and 6),

$$\frac{\Delta_{[\rho t]}}{[\rho t]} = \frac{[\mu/\rho]\sigma^2_{[\rho t]}}{2[\rho t]}. \tag{8}$$

Here, the fractional error in the integrated column density also provides the fractional error in $[\mu/\rho]$, as per equation (6). The impact of the correlation depends on the range of $[\mu/\rho]$ that is probed, and so we estimate the impact by using parameters from Fig. 2 (namely $[\mu/\rho] \simeq 150$ cm^2 g^{-1}, which is the overall range of $[\mu/\rho]$ probed by the data, and $\sigma_{[\rho t]} = 0.99$ mg cm^{-2}) to give an error in the determined absolute value of $[\mu/\rho]$ of the order of 1%. To be clear: this is the error in the determined value of $[\mu/\rho]$ when the effect of the projected roughness is ignored for this nominally 10 µm thick specimen. Relatively scaled data probing a similar range of $[\mu/\rho]$ as might appear across an absorption edge would also encounter spectral distortions at this level.

This analysis shows how easy it is to overlook the effect of projected roughness, despite the fact that the effect is substantial: here over 2.5% in the high-attenuation region across the *K*-shell absorption edge for this zinc foil. At this amplitude, the effect will suppress peak amplitudes affecting the fitted XAS parameters and the amplitude-reduction factor S_0^2.

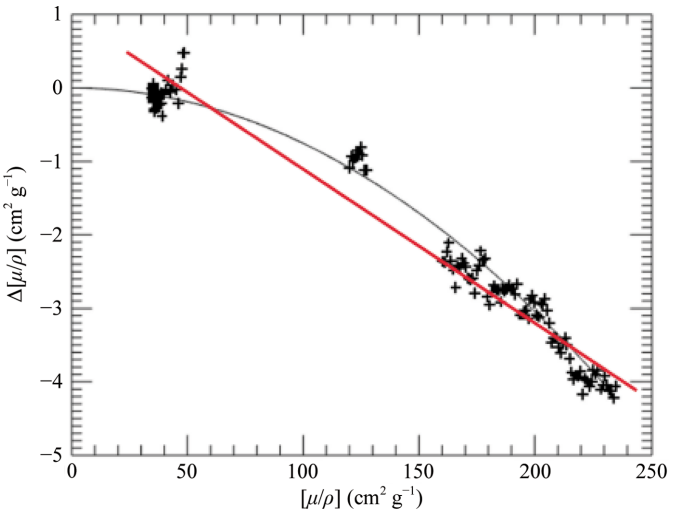

Figure 2
Difference between the measured values of the mass attenuation coefficient $\Delta_{[\mu/\rho]}$ for the 10 µm foil and the 50 µm foil as a function of mass attenuation coefficient. Projected roughness is shown here as a quadratic variation with $[\mu/\rho]$; incorrect estimation of integrated column density $[\rho t]$ would show as a linear variation. It is clear that the two effects are strongly correlated, and one must be careful to probe a suitable range of $[\mu/\rho]$. This fit determines the projected roughness to be $\sigma_{[\rho t]} = 0.99 \pm 0.004$ mg cm^{-2}, corresponding to a surprising $\sigma_t = 1.392 \pm 0.006$ µm for this nominal 10 µm thick foil. The red linear trend is discussed in the text.

6. Discussion

6.1. When will projected roughness effects be prominent?

In the last stage of equation (5) we have refactored the terms to illuminate the dependencies. As there are three correlated terms in the equation, each refactoring provides insight under certain experimental conditions and data clustering. The effect of projected roughness is significant when $[\mu/\rho]$ is high and when $[\rho t]$ is low. Interestingly, optimization of the measurement statistic (see, for example, Nordfors, 1960) typically makes these correlated: high $[\mu/\rho]$ naturally corresponds to low $[\rho t]$, *i.e.* thin specimens, with the consequence that the fractional impact increases quadratically with increasing $[\mu/\rho]$ when a fixed attenuation value is maintained.

As well as at absorption edges, the mass attenuation coefficient $[\mu/\rho]$ increases in two directions of parameter space: with reducing X-ray energy and increasing atomic number. Therefore, this effect will be particularly relevant for the significant number of tender or intermediate-energy XAS beamlines that have been developed in recent years; see, for example, Northrup (2019) and Mosselmans *et al.* (2009).

6.2. Measurement accuracy impacting tests of atomic theory

Fig. 3 shows the fractional differences between two independent tabulations of the mass attenuation coefficients, FFAST (Chantler, 1995, 2000; Chantler *et al.*, 2000) and XCOM (Berger & Hubbell, 1987, 1990; Berger *et al.*, 1999), from National Institute of Standards and Technology (2003). It is clear that the discrepancies are greatest at the *L* and *M* edges of elements with high atomic number *Z*, in the 1–3 keV

region. Challengingly, this is exactly where the projected roughness effect is greatest. Therefore, any measurement that attempts to resolve the discrepancies in Fig. 3 will need to pay particular attention to the impact of projected roughness.

6.3. Spectroscopy

Although the absolute accuracy of data for testing atomic theory is essential, the case for other methods tolerant to relatively scaled data is less obvious, and will depend on the data normalization, the analytical treatment and the inference that is required from the data. Many XAS investigations, for example, follow a process of normalization in which the pre-edge baseline is subtracted and the edge step is scaled to unit height. Whilst the robustness of this analysis lends such approaches great power, it also automatically distorts and scales the oscillation amplitudes (see Chantler, 2024*a*,*b*). The first-order effects of roughness will add to this scaling error and affect correlations between fitting parameters. Whilst such normalization is insensitive to a linear scaling, the effects resulting from projected roughness will impact data with uncorrectable systematic errors that can greatly reduce their acuity.

6.4. Future work

The concept of projected roughness developed in this chapter is new and has no current representation in the literature. While it is the correct parameter for this treatment, there are potentially many other uses that it might be put to and other insights that it might provide. It is worthwhile briefly exploring some avenues for development. The projected roughness is sensitive to impacts from both surfaces and internal structure. However, while methods for the statistical characterization of surfaces are extremely well developed, the statistical characterization of unresolved internal structure is not so well known. The method might be used, for example, to characterize deposition material densities that can be critically dependent on deposition parameters in, for example, evaporation and sputter-coating.

A measurement scheme that performs roughness determination at various probe sizes could perhaps isolate various length scales and thereby various contributions to projected roughness. Surface measurements could characterize these aspects of roughness to isolate and thus investigate internal contributions to projected roughness. We estimate that a rich domain of application for the projected roughness could arise by combining it with existing studies of surface roughness. Surface roughness has an extremely strong effect on reflection (Ehrenberg, 1949) and many experiments exploiting reflection must use super-polished samples. Surface roughness at the scale of the wavelength can lead to major changes in the amounts of specular and diffuse reflected X-rays (Sinha *et al.*, 1988). Hence, detailed studies of X-ray mirrors are able to resolve surface roughness down to the ångström level (Spiller *et al.*, 1993). Related applications that require a similarly careful treatment of roughness are X-ray multilayers (Stearns, 1992), waveguides (Lee *et al.*, 2000) and capillaries (Vincze *et al.*, 1998). Some previous studies have measured the surface roughness of polished samples by fitting a theoretical model to the wavelength dependence (Bennett, 1963) or angular dependence (Hornstrup *et al.*, 1990; Hogrefe & Kunz, 1987; Braslau *et al.*, 1985) of the intensity of the X-rays scattered from the surface. These X-ray techniques can investigate the surface roughness in the range from 5 to 50 Å (Dabagov *et al.*, 2002). However, this successful grazing-incidence approach can be affected by errors in the constituent form factors and densities, and especially in the collimation of the beam and any meniscus or strain in the target sample. Notice that this grazing technique is unsuited for projected roughness or for transmission or fluorescence measurements, and that it can only measure the roughness of the front, polished surface and only the first few atomic layers. Roughness in reflection and fluorescence is discussed in these publications and the references therein, and is a significant source of systematic errors in fluorescence. In contrast, absorption approaches can be free of these limitations.

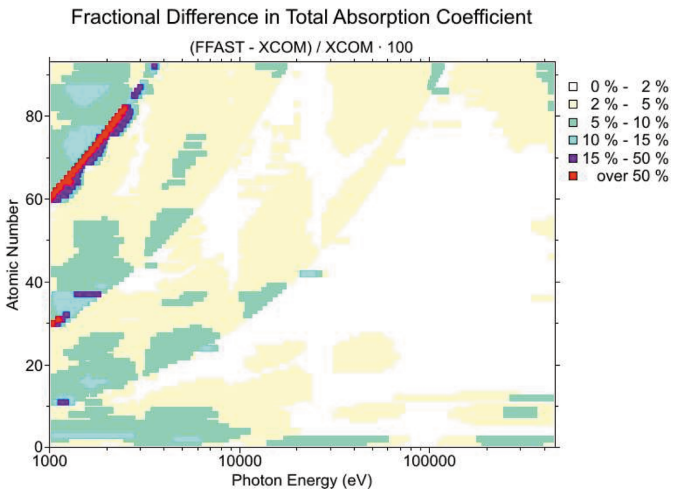

Figure 3
Comparison of the results of two theoretical tabulations of the mass attenuation coefficients identifies significant discrepancies in the 1–3 keV low-energy region, just above the *L* and *M* edges of heavy atoms, where attenuation is high and specimen thinness will almost certainly encounter roughness effects. Reproduced from https://physics.nist.gov/PhysRefData/Note/fig1.html.

7. Conclusion and challenges

Projected roughness is present in any solid sample and in the form (shape) of the mount containing liquid samples, and can affect absorption measurements by several percent. Techniques have been developed to measure and investigate these and are recommended for accurate measurement. This approach has the ability to probe surface roughness and is the first technique that can investigate 'internal' roughness. It is nondestructive and works equally well with large and small measurement areas. It can be particularly important for the determination of edge and near-edge and pre-edge features, where roughness has the greatest impact. When fingerprinting using LCF or PCA methods, the change in shape and structure

can misidentify components, local structures, oxidation states or geometries.

However, the proposed technique is not 'standard'. It requires multiple samples (Chantler, 2024*c*) and preferably a reference standard (*i.e.* a typically thicker, low-roughness foil reference; Chantler, 2024*d*). It requires the careful measurement of statistics and dark current and blank measurements (Chantler, 2024*e*). It requires measurement across significant ranges of mass attenuation coefficient, so is most effective either across an absorption edge or XANES region, or at lower X-ray energies subject to the X-ray penetrating through the sample. A beamline could be optimized for such measurement down to a small level of roughness and this could be at an XAS, X-ray fluorescence microscopy or soft or tender X-ray beamline. Indeed, it could be used as a dedicated resource supplemental to adjacent beamlines. Current results show that the projected roughness is observable, measurable and significant at third-generation XAS beamlines. Combined with normal profilometry or other surface measurements, and combined with X-ray mapping of samples to observe rolling structure and structure across the sample, this technique is able to observe and measure the effect of projected roughness inside the X-ray beam footprint on a sample. X-ray absorption projected roughness measurements show great potential.

References

Bennett, H. (1963). *J. Opt. Soc. Am.* **53**, 1389–1394.

Berger, M. J. & Hubbell, J. H. (1987). *XCOM: Photon Cross Sections on a Personal Computer*. National Bureau of Standards Report 87-3597. Gaithersburg: National Institute of Standards and Technology

Berger, M. J. & Hubbell, J. H. (1990). *NIST X-ray and Gamma-ray Attenuation Coefficients and Cross Sections Database.* NIST Standard Reference Database 8. Gaithersburg: National Institute of Standards and Technology.

Berger, M. J., Hubbell, J. H., Seltzer, S. M., Coursey, J. S. & Zucker, D. S. (1999). *XCOM: Photon Cross Sections Database.* https://physics.nist.gov/xcom.

Boster, T. A. (1973). *J. Appl. Phys.* **44**, 3778–3781.

Braslau, A., Deutsch, M., Pershan, P. S., Weiss, A. H., Als-Nielsen, J. & Bohr, J. (1985). *Phys. Rev. Lett.* **54**, 114–117.

Bridges, F. (2024). *Int. Tables Crystallogr. I*, ch. 3.13, 370–374.

Bunker, G. (2010). *Introduction to XAFS: A Practical Guide to X-ray Absorption Fine Structure Spectroscopy.* Cambridge University Press.

Bunker, G. (2024*a*). *Int. Tables Crystallogr. I*, ch. 3.12, 365–369.

Bunker, G. (2024*b*). *Int. Tables Crystallogr. I*, ch. 3.45, 567–571.

Chantler, C. T. (1995). *J. Phys. Chem. Ref. Data*, **24**, 71–643.

Chantler, C. T. (2000). *J. Phys. Chem. Ref. Data*, **29**, 597–1056.

Chantler, C. T. (2024*a*). *Int. Tables Crystallogr. I*, ch. 5.6, 659–663.

Chantler, C. T. (2024*b*). *Int. Tables Crystallogr. I*, ch. 5.7, 664–671.

Chantler, C. T. (2024*c*). *Int. Tables Crystallogr. I*, ch. 3.46, 572–573.

Chantler, C. T. (2024*d*). *Int. Tables Crystallogr. I*, ch. 5.12, 687–689.

Chantler, C. T. (2024*e*). *Int. Tables Crystallogr. I*, ch. 4.7, 624–630.

Chantler, C. T., Olsen, K., Dragoset, R., Kishore, A., Kotochigova, S. & Zucker, D. (2000). *X-ray Form Factor, Attenuation and Scattering Tables*, version 2.0. NIST Standard Reference Database 66. Gaithersburg: National Institute of Standards and Technology.

Chantler, C. T., Tran, C. Q., Barnea, Z., Paterson, D., Cookson, D. J. & Balaic, D. X. (2001). *Phys. Rev. A*, **64**, 062506.

Chantler, C. T., Tran, C. Q. & Cookson, D. J. (2004). *Phys. Rev. A*, **69**, 042101.

Dabagov, S. B., Marcelli, A., Cappuccio, G. & Burattini, E. (2002). *Nucl. Instrum. Methods Phys. Res. B*, **187**, 169–177.

de Jonge, M. D. (2005). PhD thesis. University of Melbourne, Australia.

de Jonge, M. D., Barnea, Z., Tran, C. Q. & Chantler, C. T. (2004*a*). *Meas. Sci. Technol.* **15**, 1811–1822.

de Jonge, M. D., Barnea, Z., Tran, C. Q. & Chantler, C. T. (2004*b*). *Phys. Rev. A*, **69**, 022717.

de Jonge, M. D., Tran, C. Q., Chantler, C. T., Barnea, Z., Dhal, B. B., Cookson, D. J., Lee, W. & Mashayekhi, A. (2005). *Phys. Rev. A*, **71**, 032702.

de Jonge, M. D., Tran, C. Q., Chantler, C. T., Barnea, Z., Dhal, B. B., Paterson, D., Kanter, E. P., Southworth, S. H., Young, L., Beno, M. A., Linton, J. A. & Jennings, G. (2007). *Phys. Rev. A*, **75**, 032702.

De Panfilis, S. & Bardelli, F. (2024). *Int. Tables Crystallogr. I*, ch. 4.3, 600–605.

Ehrenberg, W. (1949). *J. Opt. Soc. Am.* **39**, 741–746.

Ekanayake, R. S. K., Chantler, C. T., Sier, D., Schalken, M. J., Illig, A. J., de Jonge, M. D., Johannessen, B., Kappen, P. & Tran, C. Q. (2021*a*). *J. Synchrotron Rad.* **28**, 1476–1491.

Ekanayake, R. S. K., Chantler, C. T., Sier, D., Schalken, M. J., Illig, A. J., de Jonge, M. D., Johannessen, B., Kappen, P. & Tran, C. Q. (2021*b*). *J. Synchrotron Rad.* **28**, 1492–1503.

Glover, J. L., Chantler, C. T., Barnea, Z., Rae, N. A. & Tran, C. Q. (2010). *J. Phys. B At. Mol. Opt. Phys.* **43**, 085001.

Glover, J. L., Chantler, C. T. & de Jonge, M. D. (2009). *Phys. Lett. A*, **373**, 1177–1180.

Goulon, J., Goulon-Ginet, C., Cortes, R. & Dubois, J. M. (1982). *J. Phys. Fr.* **43**, 539–548.

Hogrefe, H. & Kunz, C. (1987). *Appl. Opt.* **26**, 2851–2859.

Hornstrup, A., Christensen, F., Jespersen, E., Henriksen, U. & Schnopper, H. (1990). *Opt. Eng.* **29**, 745.

Lee, K. K., Lim, D. R., Luan, H.-C., Agarwal, A., Foresi, J. & Kimerling, L. C. (2000). *Appl. Phys. Lett.* **77**, 1617–1619.

Mosselmans, J. F. W., Quinn, P. D., Dent, A. J., Cavill, S. A., Moreno, S. D., Peach, A., Leicester, P. J., Keylock, S. J., Gregory, S. R., Atkinson, K. D. & Rosell, J. R. (2009). *J. Synchrotron Rad.* **16**, 818–824.

National Institute of Standards and Technology (2003). *Note on NIST X-ray Attenuation Databases*. Gaithersburg: National Institute of Standards and Technology. https://www.nist.gov/pml/note-nist-x-ray-attenuation-databases.

Nordfors, B. (1960). *Ark. Fys.* **18**, 37–47.

Northrup, P. (2019). *J. Synchrotron Rad.* **26**, 2064–2074.

Sinha, S., Sirota, E., Garoff, S. & Stanley, H. (1988). *Phys. Rev. B*, **38**, 2297–2311.

Spiller, E., Stearns, D. G. & Krumrey, M. (1993). *J. Appl. Phys.* **74**, 107–118.

Stearns, D. G. (1992). *J. Appl. Phys.* **71**, 4286–4298.

Tran, C. Q., Barnea, Z., de Jonge, M. D., Dhal, B. B., Paterson, D., Cookson, D. J. & Chantler, C. T. (2003). *X-ray Spectrom.* **32**, 69–74.

Tran, C. Q., Chantler, C. T., Barnea, Z. & de Jonge, M. D. (2004). *Rev. Sci. Instrum.* **75**, 2943–2949.

Vincze, L., Janssens, K., Adams, F., Rindby, A. & Engström, P. (1998). *Rev. Sci. Instrum.* **69**, 3494–3503.